



ASAS-SN search for optical counterparts of gravitational-wave events from the third observing run of Advanced LIGO/Virgo

T. de Jaeger¹  B. J. Shappee,¹  C. S. Kochanek,^{2,3} K. Z. Stanek,^{2,3} J. F. Beacom,^{2,3,4}

T. W.-S. Holoién,⁵  Todd A. Thompson¹  A. Franckowiak⁶ and S. Holmbo⁷

¹*Institute for Astronomy, University of Hawaii, 2680 Woodlawn Drive, Honolulu, HI 96822, USA*

²*Department of Astronomy, The Ohio State University, 140 West 18th Avenue, Columbus, OH 43210, USA*

³*Center for Cosmology and AstroParticle Physics (CCAPP), The Ohio State University, 191 West Woodruff Avenue, Columbus, OH 43210, USA*

⁴*Department of Physics, The Ohio State University, 191 West Woodruff Avenue, Columbus, OH 43210, USA*

⁵*The Observatories of the Carnegie Institution for Science, 813 Santa Barbara Street, Pasadena, CA 91101, USA*

⁶*Fakultät für Physik und Astronomie, Ruhr-Universität Bochum, D-44780 Bochum, Germany*

⁷*Department of Physics and Astronomy, Aarhus University, Ny Munkegade 120, DK-8000 Aarhus C, Denmark*

Accepted 2021 October 25. Received 2021 October 4; in original form 2021 August 9

ABSTRACT

We report on the search for electromagnetic counterparts to the nine gravitational-wave events with a >60 per cent probability of containing a neutron star during the third observing run (O3) of the Laser Interferometer Gravitational-Wave Observatory (LIGO)–Virgo Collaboration (LVC) with the All-Sky Automated Survey for SuperNovae (ASAS-SN). No optical counterparts associated with a gravitational-wave event were found. However, thanks to its network of telescopes, the average area visible to at least one ASAS-SN site during the first 10 h after the trigger contained ~ 30 per cent of the integrated source location probability. Through a combination of normal operations and target-of-opportunity observations, ASAS-SN observations of the highest probability fields began within 1 h of the trigger for four of the events. After 24 h, ASAS-SN observed >60 per cent of total probability for three events and >40 per cent for all but one of the events. This is the largest area coverage to a depth of $g = 18.5$ mag from any survey with published coverage statistics for seven of the nine events. With its observing strategy, five sites around the world, and a large field of view, ASAS-SN will be one of the leading surveys to optically search for nearby neutron star mergers during LVC fourth observation run (O4).

Key words: gravitational waves – black hole mergers – neutron star mergers.

1 INTRODUCTION

Since the beginning of astronomy, we have used electromagnetic (EM) radiation to explore and understand our Universe. Gravitational waves (GWs) opened a new window for astronomy with the first-ever direct observation of GW on 2015 September 14 by two detectors of the Laser Interferometer Gravitational-Wave Observatory (LIGO; Aasi et al. 2015; Abbott et al. 2016). Since this first GW detection, ~ 70 events have been observed, with a majority due to merging black holes (BH–BH; Abbott et al. 2019, 2021). In classical general relativity, BH–BH mergers are generally not expected to have EM counterparts (Abbott et al. 2016). No confirmed counterparts have been detected for any of BH–BH mergers seen to date (but see Graham et al. 2020 for a possibility), although several theoretical studies have suggested possible EM emission mechanisms (e.g. Palenzuela, Lehner & Yoshida 2010; Moesta et al. 2012).

Unlike BH–BH mergers, binary neutron star (BNS) merger mechanisms are expected to yield an optical counterparts powered by the radioactive decay of rapid neutron capture process (r-process)

elements synthesized in the merger ejecta (Li & Paczyński 1998; Metzger et al. 2010) or by the cooling of shock-heated material around the neutron star (NS; Piro & Kollmeier 2018). On 2017 August 17, the LVC detected the first and best example of a BNS merger: GW170817 (Abbott et al. 2017a). Only two seconds after its detection, a short gamma-ray burst (GRB 170817A) was detected (Connaughton et al. 2017; Goldstein et al. 2017). GRB 170817A was followed by the discovery of the optical counterpart Swope Supernova Survey 17a [SSS17a (AT 2017gfo)] ~ 11 h later in the galaxy NGC 4993 (Coulter et al. 2017) and later confirmed by others teams (Abbott et al. 2017c; Arcavi et al. 2017; Covino et al. 2017; Díaz et al. 2017; Drout et al. 2017; Kilpatrick et al. 2017; Lipunov et al. 2017; McCully et al. 2017; Pian et al. 2017; Shappee et al. 2017; Smartt et al. 2017; Soares-Santos et al. 2017; Troja et al. 2017; Utsumi et al. 2017; Valenti et al. 2017). The combination of EM and GW information on the BNS can be used to constrain the mass and the radii of NS (Margalit & Metzger 2017) or their equation of state (Bauswein & Janka 2012; Annala et al. 2018). Also, observations of the optical–infrared (IR) ‘kilonova’ counterpart (Chornock et al. 2017; Cowperthwaite et al. 2017; Drout et al. 2017; Kilpatrick et al. 2017; Nicholl et al. 2017; Shappee et al. 2017; Valenti et al. 2017; Villar et al. 2017) provided the first observational confirmation that NS mergers produce the majority of the r-process elements heavier

* E-mail: dejaeger@hawaii.edu (TdJ); shappee@hawaii.edu (BJS)

† NHFP Einstein fellow.

than iron (Burbidge et al. 1957; Cameron 1957; Kasen et al. 2017; Pian et al. 2017; Metzger 2019). They also permit tests of theoretical kilonova models. For example, Drout et al. (2017) showed that the temperatures cooled from 10 000 to 5100 K in between 12 and 36 h after the event, confirming model predictions. Also, Shappee et al. (2017) used spectra taken 11.76 and 12.72 h after the merger to show that the photosphere was expanding at $\sim 0.3c$.

Mergers with optical counterparts can also be used as standard sirens, allowing source distances to be measured directly (Schutz 1986). From only a single EM GW counterpart detection (GW170817), Abbott et al. (2017b) derived a Hubble constant of 70_{-8}^{+12} km s $^{-1}$ Mpc $^{-1}$. Finally, any arrival time differences between the EM and GW signals test for propagation velocity differences that probe the nature of dark energy and can rule out theoretical models (Ezquiaga & Zumalacárregui 2017; Sakstein & Jain 2017; Rubin et al. 2020).

Advanced LIGO (Aasi et al. 2015) and Advanced Virgo (Acernese et al. 2015) started their third observing run (O3) to search for GW sources in 2019 April. Even though the hunt was stopped a month early due to the COVID-19 pandemic, an increase in sensitivity during O3 (Buikema et al. 2020) allowed the discovery of more than 56 events in 330 d, including nine with a high probability of having at least one NS. Unlike first observing run (O1) and second observing run (O2), LVC O3 had a public alert system that automatically sent alerts within minutes of the GW detections, allowing all astronomers to search for EM counterparts. Following the successful observations of SSS17a (GW170817), many surveys participated in the searches for GW optical counterparts during the LVC O3 run. These surveys include: the All-Sky Automated Survey for SuperNovae (ASAS-SN; Shappee et al. 2014), the Asteroid Terrestrial-impact Last Alert System (ATLAS; Tonry et al. 2018), the Deca-Degree Optical Transient Imager (DDOTI; Becerra et al. 2021), the Dark Energy Camera (DECam; Flaugher et al. 2015), the Electromagnetic counterparts of gravitational wave sources at the Very Large Telescope (ENGRAVE; Levan & Jonker 2020), the Gravitational-wave Optical Transient Observer (GOTO; Dyer et al. 2018), the Global Rapid Advanced Network Devoted to the Multi-messenger Addicts (GRANDMA) survey (Antier et al. 2020), the Katzman Automatic Imaging Telescope (KAIT; Filippenko et al. 2001), the Panoramic Survey Telescope and Rapid Response System (Pan-STARRS; Chambers et al. 2016), the Searches After Gravitational waves Using ARizona Observatories (SAGUARO; Lundquist et al. 2019), SkyMapper (Chang et al. 2021), and the Zwicky Transient Facility (ZTF; Bellm et al. 2019).

During the LVC O3, more than 1500 Gamma-ray Coordinates Network (GCN) circulars were published to report EM counterpart searches and potential candidates. Approximately 60 observatories were involved in the optical follow-ups, yielding ~ 388 candidate counterparts (Coughlin 2020). Unfortunately, no optical counterparts were linked to a GW event. This shows the uniqueness of SSS17a (GW170817; Abbott et al. 2017a): a rare 40_{-8}^{+14} Mpc NS event leading to a localization area of only 28 deg 2 . In comparison, the LVC O3 events with a > 60 per cent probability of containing a NS had an average 90 per cent confidence localization of ~ 4700 deg 2 and an average distance of ~ 330 Mpc (see Table 1). This explains why searches for EM counterparts in O3 were challenging and unsuccessful.

Several groups participating in searches for GW optical counterparts during LVC O3 run have already published an overview of their strategy: GOTO (Gompertz et al. 2020), GRANDMA (Antier et al. 2020), SAGURO (Paterson et al. 2021), and ZTF (Coughlin et al. 2020a,b; Kasliwal et al. 2020a). These studies describe both

Table 1. Characteristics of the LVC events triggered by ASAS-SN during the O3 run. In the first column the event name, followed by its discovery date in UTC are listed. In column 3, we list the sky area in deg 2 of the search region. In columns 4 and 5, we list the distance in Mpc together with its uncertainty and their false alarm rate (FAR) in yr $^{-1}$. In column 6, we list the probability that the lighter compact object has a mass $< 3 M_{\odot}$, while columns 7–11 give the classification probabilities of the GW signal. Column 12 is the fraction of the probability that ASAS-SN covered in 24 h. Finally, GCN circular reference is given in the last column. All the parameters were taken from the Gravitational-Wave Candidate Event Database (<https://gracdb.ligo.org/superevents/public/O3/>).

Event	Date (UTC)	90 per cent sky area (deg 2)	Distance (Mpc)	FAR (yr $^{-1}$)	P_{NS} (per cent)	BH-BH (per cent)	NSBH (per cent)	Classification probability BNS (per cent)	MassGap (per cent)	Terrestrial (per cent)	Prob. cov (per cent)	GCN	
S190425z	2019 Apr 25, 08:18:05	10183	15.5 (45)	1.43×10^{-5}	>99	<1	<1	>99	<1	0	67	24168	
S190426c	2019 Apr 26, 15:21:55	1262	375 (108)	0.61	>99	<1	13	49	24	14	85	24237	
S190901ap	2019 Sept 1, 23:31:01	13613	242 (81)	0.22	>99	<1	86	<1	14	58	25606		
S190910d	2019 Sept 10, 01:26:19	3829	606 (197)	0.12	>99	<1	98	<1	<1	2	52	25695	
S190923y	2019 Sept 23, 12:55:59	2107	438 (133)	1.51	>99	<1	68	<1	<1	32	44	25814	
S191205ah	2019 Dec 5, 21:52:08	6378	385 (164)	0.39	>99	<1	93	<1	<1	7	42	26350	
S191213g	2019 Dec 13, 04:34:08	1393	195 (59)	1.12	>99	<1	77	<1	<1	23	1	26402	
S200115j	2020 Jan 15, 04:25:09	908	331 (97)	6.61×10^{-4}	>99	<1	<1	>99	<1	63	63	26759	
S200213t	2020 Feb 13, 04:10:00	2587	224 (90)	0.56	>99	<1	63	<1	<1	37	42	27042	

individual events and the lessons learned from LVC O3 to prepare for LVC fourth observation run (O4; starting in \sim 2022 June). For example, one concern that should be addressed by the GW community is the lack of follow-up for a large number of candidates even as several candidates were classified multiple times by different groups (Coughlin et al. 2020b).

In this paper, we present a summary of the ASAS-SN observational strategy during the LVC O3 run and show that, thanks to our five sites spread over the world, the majority of the events were observable from at least one ASAS-SN site soon after their discovery. In Section 2, we describe ASAS-SN characteristics and our observational strategy. In Section 3, we present all the LVC events for which ASAS-SN obtained data during the O3 run. Finally, we discuss our results in Section 4 and conclude in Section 5.

2 THE ASAS-SN STRATEGY

ASAS-SN is the first and still the only ground-based survey to map the entire visible sky daily to a depth of $g = 18.5$ mag (Shappee et al. 2014; Kochanek et al. 2017). Currently, ASAS-SN is composed of five stations: Brutus, the original ASAS-SN unit, located on Haleakala in Hawaii (USA); Cassius and Paczynski, both situated at Cerro Tololo International Observatory (CTIO) in Chile; Leavitt at McDonald Observatory in Texas (USA), and finally Payne-Gaposchkin at the South African Astrophysical Observatory (SAAO) in Sutherland, South Africa. All units are hosted by the Las Cumbres Observatory Global Telescope (LCOGT) network (Brown et al. 2013) and consist of four 14-cm aperture Nikon telephoto lenses, each with a 4.47×4.47 field of view. ASAS-SN survey operations are composed of three dithered 90-s exposures using a g -band filter (all five units) with ~ 15 s of overheads between each image, for a total of 315 s per field. Thanks to the five stations, the instantaneous field of view is roughly 360 deg^2 . Note that we will refer to the estimated location of a GW event as the search region. In practice, the search region is defined by probabilities, and unless otherwise specified, we are considering the region enclosing 90 per cent of the probability for the event location. We try to observe fields in order of their average probability of containing the event.

In Fig. 1, we show the fraction of the search region visible to ASAS-SN as a function of time for all the LVC O3 events with a $P_{\text{NS}} > 60$ per cent probability that at least one of the compact objects is a NS. For all events, a large percentage of the search region (~ 30 per cent) is visible at least once within the first 24 h. For example, less than 1 h after the LVC alert, over 35 per cent of the search region was visible for five events, while only three were under 15 per cent, and one region was not visible at all. This allows ASAS-SN to respond promptly to almost all the LVC alerts independent of the time or localization.

To maximize our chance of observing an optical counterpart of GW sources, ASAS-SN has a Target-of-Opportunity (ToO) mode to enable rapid imaging follow-up. Our automated system receives all LVC alerts using the GCN protocol along with the IceCube real-time alerts (Aartsen et al. 2017). We follow only the GW events with a $P_{\text{NS}} > 60$ per cent or nearby BH–BH (distance < 100 Mpc) as theoretical studies have suggested possible faint EM emission mechanisms. All the events with a > 40 per cent probability of being terrestrial are discarded as they generally end up being false alarms. For all the interesting events, a list of the 30 pointings with the highest localization probability is automatically generated and the ToO observations start. Each pointing corresponds to a total of 70 deg^2 after accounting for the four camera/field overlaps. We limit our selection to 30 pointings as this is generally sufficient to

cover more than 70 per cent of the search region and normal survey operations cover the entire visible sky daily regardless. After the first hour in ToO mode, the routine survey is optimized to increase the cadence of the fields in the search region. For example, during the LVC O3 run, pointings within the highest probability region were observed 4–5 times in 24 h. The images are processed using the ISIS image subtraction package (Alard & Lupton 1998; Alard 2000), *SExtractor* (Bertin & Arnouts 1996) to detect new sources, and a combination of parameters cuts, a random forest classifier, and a convolutional neural network to isolate real sources. Known variables, asteroids, and transients are automatically flagged. The remaining candidates are checked by eye in near real-time. Finally, the interesting optical counterpart candidates are reported to GCN. As described in Section 3, no good candidates were detected and reported for the LVC O3.

A schematic summary of the strategy is displayed in Fig. 2.

Finally, as a galaxy-targeted strategy is more suitable for telescopes with a small field of view, a list of nearby galaxies (< 100 Mpc) is sent simultaneously to a group of dedicated amateur astronomers with whom ASAS-SN collaborates during normal operation to confirm ASAS-SN discoveries. Nearby galaxies are selected from the Gravitational Wave Galaxy Catalogue (White, Daw & Dhillon 2011), a catalogue of 53 255 galaxies with high completeness to 100 Mpc and ranked by the probability that a particular galaxy hosts a GW event (P_{gal}). The final probability is taken from Coulter et al. (2017) and depends on the search region (P_{2D}), the galaxy and event distances (D_{gal} and D_{LVC} , respectively), the galaxy luminosity (\tilde{L}_B), and a normalization factor (k):

$$P_{\text{gal}} = k^{-1} \times \tilde{L}_B \times P_{\text{2D}} \times \left(1 - \text{erf} \left(\frac{|D_{\text{gal}} - D_{\text{LVC}}|}{\sigma_{D_{\text{gal}}}^2 + \sigma_{D_{\text{LVC}}}^2} \right) \right). \quad (1)$$

Given the completeness of the Gravitational Wave Galaxy Catalogue and the large distance estimates for all of the LVC O3 events, it is unsurprising that the amateur astronomers did not find anything this cycle. They will continue to search in future observing runs.

3 EW FOLLOW-UP

In this section, we describe each of the nine events announced for the LVC O3 run that passed our selection criterion as described in Section 2. For the nine events, all having a $P_{\text{NS}} > 60$ per cent probability of containing a NS, we obtained data from a combination of normal operations and an optimization of our observational strategy to observe the search region with a higher cadence. For all the events presented in this section, we use the initial localization map from the BAYESian TriAngulation and Rapid localization (BAYESTAR; Singer & Price 2016). A list of those events together with their principal characteristics is given in Table 1. Note that from the nine events, only two events (S190425z and S190426c) were published in the Gravitational-Wave Transient Catalog 2 (GWTC-2; Abbott et al. 2021), three events (S190901ap, S190910d, and S190923y) were disseminated via GCNs but were not recovered in GWTC-2, and four events (S191205ah, S191213g, S200115j, and S200213t) were detected during the second half of the LVC O3 run and their final states have yet to be reported.

3.1 S190425z

S190425z was the first BNS detection of the LVC O3 run. It was detected on 2019 April 25 at 08:18:05 UTC by the Advanced

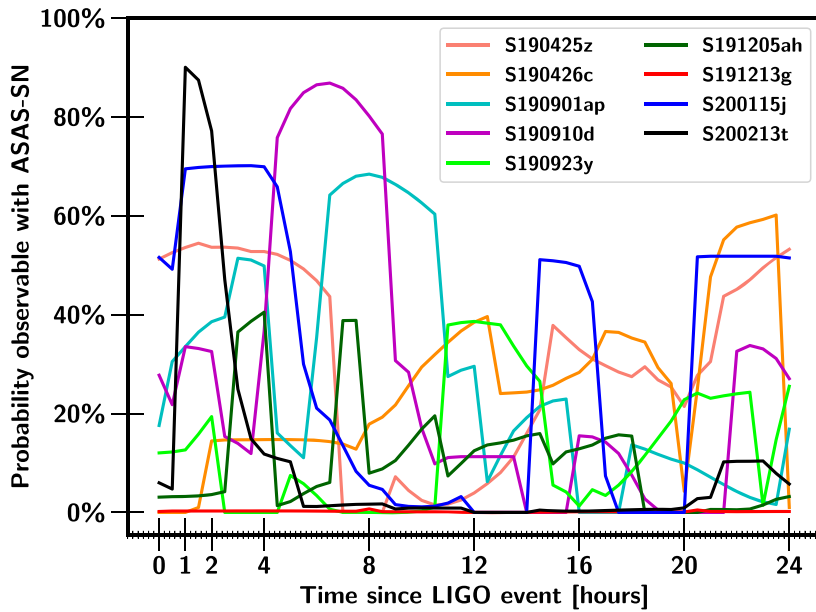


Figure 1. Instantaneous probability observable by ASAS-SN versus the time in hours since the LVC alert.

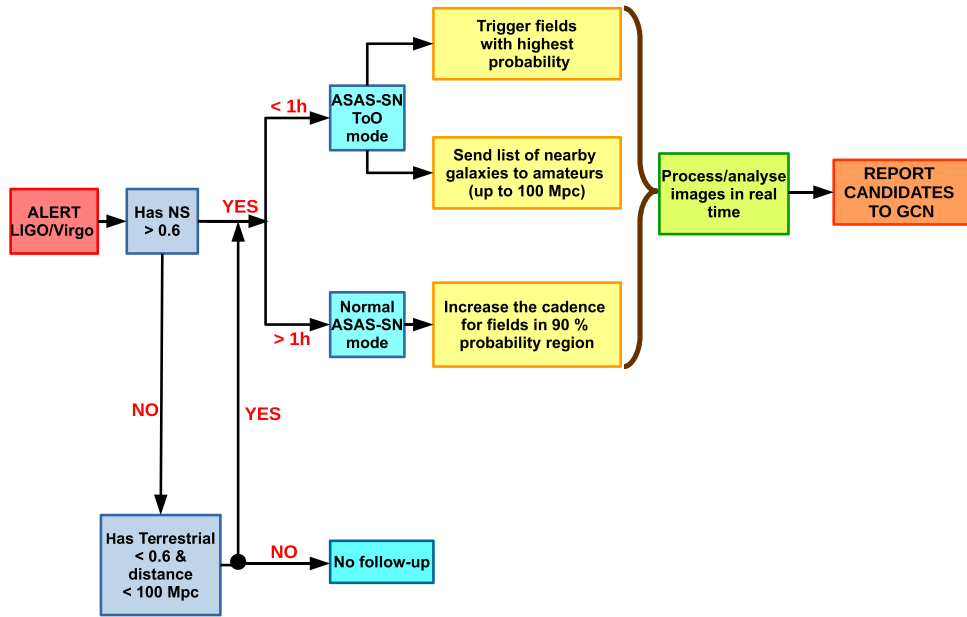


Figure 2. ASAS-SN strategy diagram. Our automated system receives a GCN LVC alert and updates the plan of observations to search for optical counterparts in only a few seconds. If the alert properties meet the triggering criteria, the list of fields/pointings to observe is automatically created and prioritized and all the images are analysed in real-time. Finally, good candidates are manually reported to GCN.

LIGO Livingston detector (LIGO Scientific Collaboration & Virgo Collaboration 2019a) with a false alarm rate (FAR) of 1 in $\sim 70\,000$ yr and a $P_{\text{NS}} > 99$ per cent probability of being a BNS. The first search region was an extended area spanning $10\,183 \text{ deg}^2$ and the estimated distance was 155 ± 45 Mpc. Because of the success of the GW170817 optical counterpart hunt and because S190425z was the first event with a high probability of having an optical counterpart, an intense follow-up campaign started a few seconds after the LVC alert, leading to a total of 120 GCN circulars, including two from ASAS-SN (Shappee et al. 2019a,b).

In Fig. 3, we show the search region covered by ASAS-SN from its five sites. The ASAS-SN response was fast and in less than 1 h after the alert, 10 per cent of the total search region was already mapped through triggered observations to a 5σ g -band limiting magnitude of ~ 18.5 mag. After 24 h, ~ 70 per cent of the integrated LVC localization probability was covered through a combination of normal operations and triggered observations. For comparison, ATLAS covered a sky region totalling of 37.2 per cent of the event's localization likelihood in ~ 6 h (McBrien et al. 2019), GOTO covered 29.6 per cent in 9 h (Steeghs et al. 2019a), Pan-STARRS

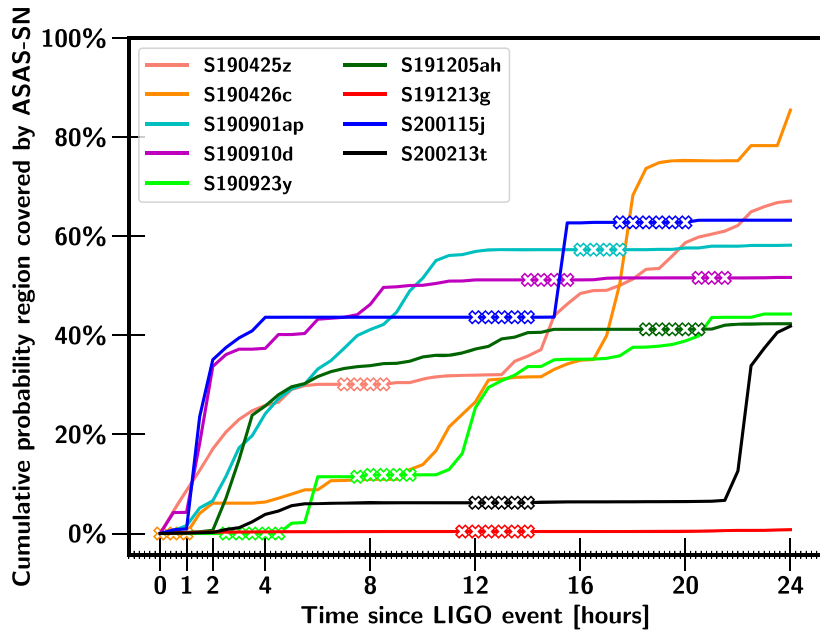


Figure 3. Cumulative probability covered by ASAS-SN (all sites) versus the time in hours since the LVC alert for the nine events. The white crosses indicate when a search region is not visible from any ASAS-SN sites due to the restrictions that (1) the Sun is at least 12° below the horizon, (2) the airmass is at most 2, (3) the hour angle is at most 5 h, and (4) that the minimum distance to the Moon is larger than 20° .

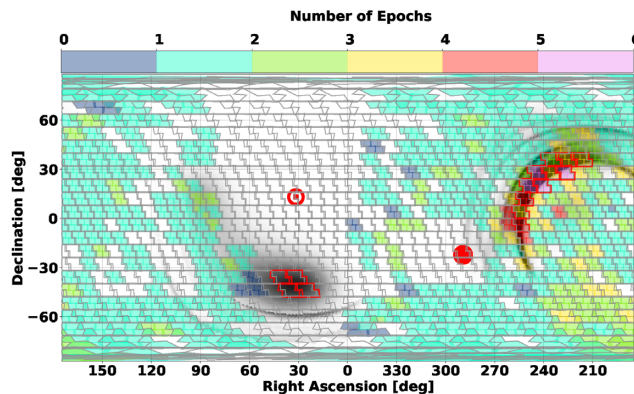


Figure 4. Plate carrée projection of the ASAS-SN data obtained in the first 24 h for S190425z. The black shaded area corresponds to the localization area and the red ASAS-SN boundaries are the fields selected to be observed immediately after the event detection. Red filled circle and \odot markers represent the position of the Moon and Sun, respectively. The colour of the field shows the number of epochs observed.

covered 28 per cent in ~ 19 h (Smith et al. 2019), and ZTF covered 21 per cent in ~ 28 h (Coughlin et al. 2020a). Fig. 4 shows the ASAS-SN coverage for the 24 h. As we can see, the normal ASAS-SN observation mode was optimized to increase the cadence for the fields within the search region and we were able to observe those fields 5–6 times over the next day. Finally, in all the search region images taken during the first 24 h, we flagged 421 stars that had varied, nine asteroids, and zero transients.

3.2 S190426c

S190426c was detected by LVC on 2019 April 26 at 15:21:55 UTC with an FAR of 1 in ~ 1.6 yr (LIGO Scientific Collaboration &

Virgo Collaboration 2019b). The classification of the GW signal, in order of descending probability, was BNS (49 per cent), MassGap (24 per cent), terrestrial (14 per cent), NSBH (13 per cent), or BBH (< 1 per cent). MassGap refers to a binary system with at least one compact object whose mass is in the range between NS and BHs, defined as $3-5 M_\odot$. The first search region spanned ~ 1262 deg 2 and the estimated distance was 375 ± 108 Mpc. Because of the nature of the event, a large number of teams searched for an optical counterpart and ~ 70 GCN circulars were sent, including one from ASAS-SN (Shappee et al. 2019c). As seen in Figs 3 and A1, ASAS-SN mapped ~ 90 per cent of the search region in 24 h. Unlike S190425z, the first fields were observed 1.5 h after the GW detection due to Sun constraints. Of the nine events presented in this paper, S190426c is the one with the most ASAS-SN observations, with up to 13 epochs over less than 24 h for the fields within the search region. This demonstrates how we can change the ASAS-SN strategy in real-time and go deeper to discover fainter candidates. For the high-cadence fields, we reached a *g*-band limiting magnitude of ~ 19.8 mag. As with S190425z, ASAS-SN covered one of the largest areas in 24 h with respect to other major surveys: GOTO covered 54 per cent of the source location probability in 9 h but started ~ 6 h after the discovery (Steeghs et al. 2019b), while ZTF covered 75 per cent of the sky localization but in 31 h and starting 13 h after the alert (Coughlin et al. 2020a). In all the search region images taken during the first 24 h, we flagged 1931 variable stars, 79 asteroids, and one transient, a cataclysmic variable.

3.3 S190901ap

S190901ap was detected on 2019 September 1 at 23:31:01 UTC with a probability of 86 per cent to be a BNS and 14 per cent to be terrestrial (LIGO Scientific Collaboration & Virgo Collaboration 2019c). However, its large search region of 13613 deg 2 and distance of 242 ± 81 Mpc appears to have discouraged groups from searching

for an EM counterpart and only ~ 40 GCN circulars were sent. For this event, the majority of the observed fields within the search region were observed in normal operations, as seen in Fig. A2, with a median co-added g -band depth of ~ 19.1 mag and some fields reaching ~ 19.3 mag. Mostly using normal operations, ASAS-SN covered ~ 60 per cent of the search region in 24 h starting < 1 h after the LVC alert (see Fig. 3). Compared to other teams that reported their observations, ASAS-SN covered one of the largest integrated search probabilities in the first 24 h. For example, GOTO covered 28 per cent of the search region in 54 h starting ~ 0.1 h after the discovery (Ackley et al. 2019), while ZTF covered 73 per cent of the sky localization but over ~ 73 h and beginning 3.6 h after the detection (Stein et al. 2019; Coughlin et al. 2020a). In all the search region images taken during the first 24 h, we flagged 106 variable stars, three asteroids, and zero transients.

3.4 S190910d

S190910d was discovered on 2019 September 10 at 01:26:19 UTC (LIGO Scientific Collaboration & Virgo Collaboration 2019d). This event was classified as NSBH with a probability of 98 per cent (terrestrial: 2 per cent) and a false alert rate of 1 in 8 yr. Only a few teams (~ 20 GCN circulars) participated in the follow-up of this object situated at 606 ± 197 Mpc with a search region of 3829 deg^2 . ASAS-SN covered 50 per cent of the search region in 24 h (see Fig. 3). For the same object, GRANDMA covered 37 per cent in 65 h (Crisp et al. 2019), while ZTF covered 34 per cent in 1.5 h (Anand et al. 2019). As seen in Fig. A3, ASAS-SN obtained a maximum of three epochs for some fields within the search region and reached a median g -band depth of ~ 17.7 mag with a maximum of ~ 18.4 mag. In all the search region images taken during the first 24 h, we flagged 369 variable stars, zero asteroid, and zero transients.

3.5 S190923y

S190923y was detected on 2019 September 23 at 12:55:59 UTC (LIGO Scientific Collaboration & Virgo Collaboration 2019e). The classification for this event was 68 per cent NSBH, but with a high probability of being terrestrial (32 per cent). Because of a non-negligible false positive rate of 1 per 7 months, a distance of 438 ± 151 Mpc, and a search region of 2107 deg^2 , half of which was close to the Moon, only ~ 15 GCN circulars were sent. As seen in Fig. A4, ASAS-SN increased the cadence for the fields within the search region and obtained a maximum of three epochs for those fields and a median g -band depth of 18.3 mag. As seen in Fig. 3, ASAS-SN covered ~ 40 per cent of the search region in 24 h with the first fields observed starting ~ 4 h after the discovery due to observability constraints. As ASAS-SN only targets fields more than 20° from the Moon, only half of the search region was observable. In comparison, GRANDMA covered 26 per cent in 55 h starting ~ 4 h after the alert (Turpin et al. 2019). In all the search region images taken during the first 24 h, we flagged 2084 variable stars, 47 asteroids, and zero transients.

3.6 S191205ah

S191205ah was detected on 2019 December 5 at 21:52:08 UTC (LIGO Scientific Collaboration & Virgo Collaboration 2019f) with an FAR of ~ 1 per 2.5 yr. The classification was 93 per cent NSBH and 7 per cent terrestrial at a distance of 385 ± 164 Mpc. The GW candidate was poorly localized with a search region spanning 6378 deg^2 . Only a few teams participated in the EM counterpart

hunt and only ~ 30 GCN circulars were sent. Through its routine and optimized survey operations, ASAS-SN covered ~ 40 per cent of the search region in 24 h (see Fig. 3) with the first observation 2 h after the discovery. ZTF covered 6 per cent in 167 h starting ~ 11 h post-discovery (Andreoni et al. 2019a; Coughlin 2020) and GRANDMA mapped 4.8 per cent in ~ 150 h (Antier et al. 2020). Fig. A5 shows that our strategy obtained multiple epochs for the high-probability regions that were sufficiently distant from the Moon. The median g -band depth was 16.97 mag with a maximum of 18.30 mag. In all the search region images taken during the first 24 h, we flagged 101 variable stars, 37 asteroids, and zero transients.

3.7 S191213g

S191213g was detected on 2019 December 12 at 04:34:08 UTC (LIGO Scientific Collaboration & Virgo Collaboration 2019g). The classification probabilities were 77 per cent BNS and 23 per cent terrestrial. With an FAR of 1.12 yr^{-1} , a distance of 195 ± 59 Mpc, and a search region of 1393 deg^2 , S191213g was fairly well observed (~ 50 GCN circulars). However, as seen in Fig. A6, the search region was within the Sun and hour angle limit of 5 h so ASAS-SN did not observe it, leading to its 0 per cent coverage in Fig. 3. ZTF was able to cover 28 per cent of the probable region in 27 h by observing at high airmass in twilight (Andreoni et al. 2019b), while GRANDMA observed only 1 per cent over 73 h (Ducoin et al. 2019).

3.8 S200115j

S200115j was identified on 2020 January 15 at 04:23:08 UTC with an FAR of 1 per 1573 yr (LIGO Scientific Collaboration & Virgo Collaboration 2020a). It was classified as a MassGap event with a probability of 99 per cent, a distance of 331 ± 97 Mpc, and a search region spanning 908 deg^2 , one of the smallest regions in LVC O3. As seen in Fig. A7, only two-thirds of the search region was observed by ASAS-SN due to Sun constraints. Fields within the search region were targeted at a slightly higher frequency (2–4 epochs) with a median g -band depth of 17.8 mag and a maximum of 18.5 mag. For this event, ASAS-SN was among a few groups to obtain data and only ~ 30 GCN circulars were sent. As shown in Fig. 3, ASAS-SN was able to cover ~ 60 per cent of the search region in 24 h and the first fields within the search region were observed 1 h after the LVC alert. Among other teams, SAGURO observed 2.1 per cent of the LVC total probability in 24 h starting 72 h after the event (Paterson et al. 2021), ZTF scanned 22 per cent in 1 h to a depth of 21.2 mag starting 15 min after the alert (Anand et al. 2020; Coughlin 2020), and GRANDMA observed 7 per cent in 24 h starting 11 h after the event with a depth of 17 mag in clear band. In all the search region images taken during the first 24 h, we flagged 22 variable stars, 16 asteroids, and zero transients.

3.9 S200213t

The last GW candidate with a high NS probability was discovered on 2020 February 13 at 04:10:40 UTC (LIGO Scientific Collaboration & Virgo Collaboration 2020b). S200213t had an FAR of ~ 1 per 1.8 yr, a search region of 2587 deg^2 , and a distance of 224 ± 90 Mpc. For this event, the probability of a terrestrial origin was non-negligible (37 per cent), but due to the 63 per cent probability of being a BNS, several searches followed up this signal (~ 50 GCN circulars). The localization region was confined to relatively high northern latitudes, and the two northern ASAS-SN sites were not immediately able to obtain data. Haleakala Observatory was closed due to damage from

an ice storm and McDonald Observatory had bad weather during the ~ 2 h ToO period. As we can see in Fig. A8, all the fields overlapping the search region were ultimately observed. A maximum of 2–3 epochs were obtained with a median g -band depth of 18.5 mag. ASAS-SN was able to cover ~ 40 per cent of the search region, mostly between 22 and 24 h after the event. In comparison, ZTF covered 72 per cent of the area in less than 1 d to a g -band magnitude limit of ~ 20.7 mag (Kasliwal et al. 2020b), GOTO observed 54 per cent in ~ 26 h starting a few seconds after the event, and GRANDMA mapped ~ 30 per cent in ~ 44 h starting 30 min after the event. In all the search region images taken during the first 24 h, we flagged 208 variable stars, 11 asteroids, and one transient, a luminous red nova or a luminous blue variable (Kawabata 2020).

4 DISCUSSION

In Section 3, we detailed all the GW candidates with a high probability of having an optical counterpart. Like the rest of the community, we did not detect a kilonova during LVC O3. To understand why, we will first study the case of SSS17a, the only kilonova detected to date. Then we will use SSS17a-like objects as a tool to improve our observational strategy for detecting future kilonovae.

4.1 S170817a

Unfortunately, when S170817a was discovered, all the LVC alerts were private and ASAS-SN was not part of the collaboration. For this reason, ASAS-SN covered 0 per cent of the search region and the only data obtained were gathered in the normal observation mode. Because of the small 28 deg^2 size of the search region, it was contained in just five pointings and our likelihood of having randomly observed this event were small for two reasons. First, SSS17a was only observable early in the night and fields far over in either direction are less likely to be observed due to the limited amount of time available to observe them. Second, at that time, only the Brutus and Cassius sites were operational. Paczynski, Leavitt, and Payne-Gaposchkin were just coming online, obtaining their first night of data a few weeks after the event on 2017 September 2, September 20, and October 29, respectively.

However, given that LVC alerts are now public, all five sites are available, and we have observationally tested our initial strategy, we can use SSS17a-like objects to investigate how ASAS-SN should respond to future kilonova events. Fig. 5 shows a Hammer–Aitoff projection of the ASAS-SN fields superposed on the search region for SSS17a. Five pointings cover 98 per cent of the search region and just two pointings (F1251 – 22 and F1324 – 22) cover 70 per cent of the total probability. Given our strategy as described in Section 2, ASAS-SN would trigger observations of the five fields by order of probability (i.e. F1251 – 22, F1324 – 22, F1306 – 14, F1328 – 30, and F1254 – 30). This means that we would have discovered SSS17a a few seconds after the LVC alert in our second pointing, ~ 10 min after starting the hunt. For comparison, Coulter et al. (2017) – who were the first team to discover SSS17a ~ 11 h after the alert – did a galaxy-targeted search with the Swope Telescope (Las Campanas Observatory, Chile) and found SSS17a in their ninth image (the twelfth-highest probability galaxy). This means that ASAS-SN would have discovered SSS17a almost at the same time as Coulter et al. (2017) using only the Cassius site in Chile. However, with the ASAS-SN unit in South Africa (Payne-Gaposchkin), deployed 2 months after GW170817, ASAS-SN would have discovered SSS17a 4.5 h after the LVC alert instead of 10–11 h from Chile. Such

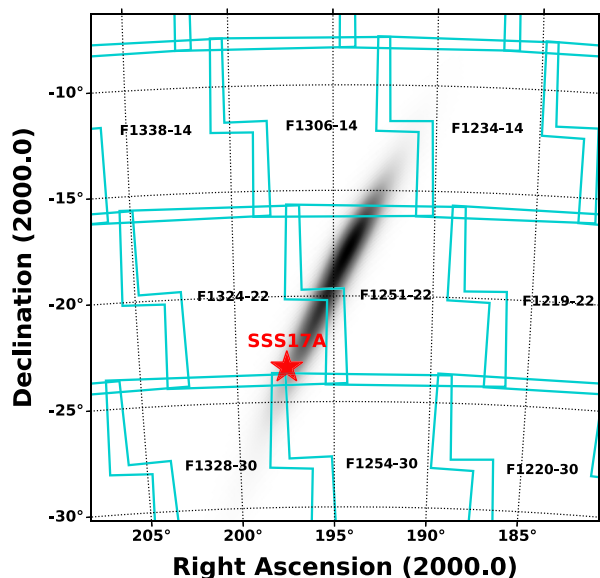


Figure 5. Hammer–Aitoff projection of the ASAS-SN fields (cyan) with the black shaded area corresponding to the search region of SSS17a. The red star represents the position of SSS17a. The names of the ASAS-SN fields are also written in black.

early data are crucial to differentiate shock cooling and radioactively powered models and to explain the blue component of the kilonova (Piro & Kollmeier 2018). It is also important to note that unlike the majority of other surveys, ASAS-SN already has deep templates over the entire sky and a ~ 10 yr of variability history.

SSS17a was easily discovered mostly thanks to its small distance (40 Mpc). In Fig. 6, we show the SSS17a g -band light curve (Andreoni et al. 2017; Arcavi et al. 2017; Coulter et al. 2017; Cowperthwaite et al. 2017; Díaz et al. 2017; Drout et al. 2017; Pian et al. 2017; Shappee et al. 2017; Smartt et al. 2017; Troja et al. 2017; Utsumi et al. 2017) not corrected for Milky Way extinction and the cocoon model from Piro & Kollmeier (2018) for distances from 40 to 200 Mpc. With ASAS-SN and an average 5σ g -band limiting magnitude of 18.5 mag for a single epoch per field (~ 5 min), SSS17a was bright enough for ASAS-SN to detect for ~ 1.5 d even with our normal survey observations. The maximum distance for a single normal survey epoch to detect an SSS17a-like source is ~ 60 –75 Mpc. However, once triggered we also increase the cadence for the fields within the source region, leading to a fainter 5σ limiting magnitude. For example, for small probability areas, it would be easy to reach 45 min of exposure time per field corresponding to a limiting magnitude of ~ 19.6 mag and the ability to detect SSS17a at a distance of ~ 120 Mpc (see also Section 4.2). SSS17a suffered from a higher than average Milky Way g -band extinction of ~ 0.4 mag (Schlafly & Finkbeiner 2011). As more than half of the sky has a lower Milky Way extinction, most future kilonovae will be less extinguished and detectable at moderately larger distances. Note that increasing the limiting magnitude will also increase the number of candidates. For all the candidates we will do a by-eye verification, perform forced aperture photometry at the same location in ASAS-SN and ATLAS data, and then announce the best candidates to the community. Ultimately, spectra are required for final confirmation and will be obtained using institutional resources of the ASAS-SN collaboration especially the soon to be robotized University of Hawaii 2.2-m telescope at Mauna Kea Observatory in Hawaii (USA).

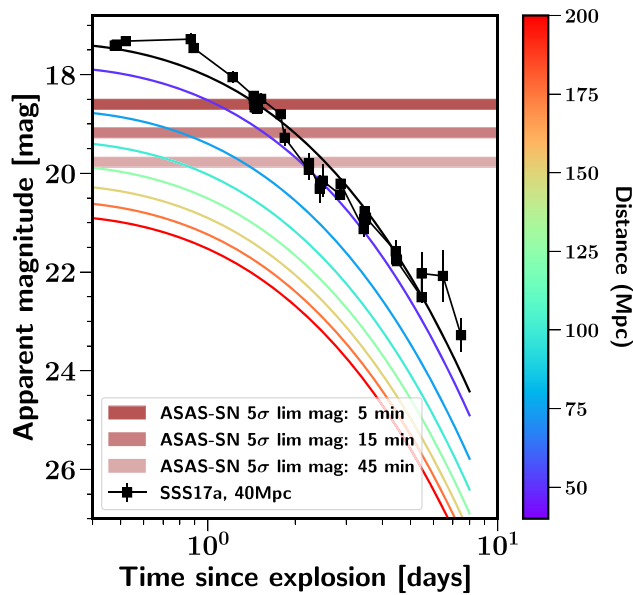


Figure 6. SSS17a *g*-band apparent magnitude evolution for different distances. The original light curve is displayed in black (40 Mpc), while the lines corresponds to the cocoon model (Piro & Kollmeier 2018) for different distances in Mpc defined by the colour bar. The three brown horizontal bands are the 5σ *g*-band limiting magnitude from ASAS-SN for exposures time per field of 5, 15, and 45 min, respectively (see Section 4.2 for more details). The *g*-band data were taken from the compilation in Villar et al. (2017) and were originally published in Andreoni et al. (2017), Arcavi et al. (2017), Coulter et al. (2017), Cowperthwaite et al. (2017), Díaz et al. (2017), Drout et al. (2017), Pian et al. (2017), Shappee et al. (2017), Smartt et al. (2017), Troja et al. (2017), and Utsumi et al. (2017).

4.2 Strategy for LVC O4

The next LVC observing run is expected to start in 2022 June with an additional detector located in Japan (Kagra). LIGO–Virgo–Kagra (LVK) detections have a predicted median search area of $33^{+4.9}_{-5.3} \text{ deg}^2$ (Abbott et al. 2020), an area similar to SSS17a. However, using a higher FAR, Petrov et al. (2021) argued that an area of $1820^{+190}_{-170} \text{ deg}^2$ is more realistic.

Because ASAS-SN already has deep reference images covering the entire sky, we can obtain longer exposure times to search for counterparts at fainter magnitudes without significant noise contribution from the reference image. Fig. 7 shows the depth of ASAS-SN *g*-band reference images. A typical reference image is composed of images totalling several hours of exposure time, with a median 5σ *g*-band limiting magnitude of 20.3 mag. Fig. 8 illustrates which events ASAS-SN should follow given its distance and search area, assuming a peak absolute magnitude like SSS17a. We assume the event is visible for 5 h from three of our five sites and that SSS17a stayed near its peak for 300 min (see Fig. 6).

For simplicity, we ignore edge effects and assume that the total field of view of ASAS-SN is entirely contained within the search region, so that each pointing covers 70 deg^2 of the search region. For the largest search areas, we can only dedicate ~ 5 min to each field to cover $\sim 12,600 \text{ deg}^2$ in one night at a depth of 18.5 mag. This would detect an SSS17a out to ~ 70 Mpc. If we observe only one field, we can reach a total exposure time of 900 min (3 sites \times 5 h) in one night. For these very long exposures, the sensitivity will be limited by the depth of the reference images and we can reach a 5σ *g*-band limiting magnitude of 20.3 mag to detect SSS17a-like object out to

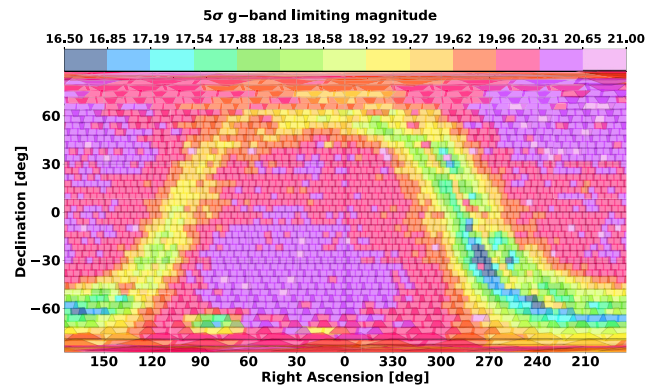


Figure 7. Plate carrée projection of the depth of ASAS-SN *g*-band reference images over the sky. The colour of the different ASAS-SN field shows the 5σ *g*-band limiting magnitude of the reference images. The median depth over all the sky is 20.3 mag.

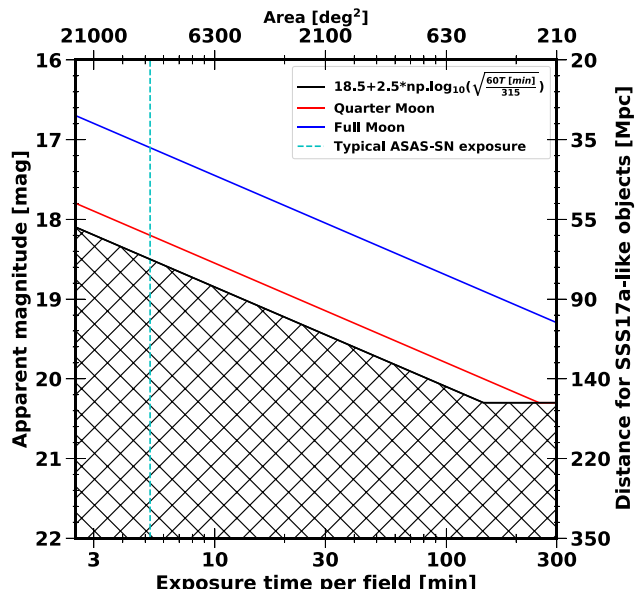


Figure 8. Apparent magnitude limits versus total exposure time in minutes. The black, red, and blue lines represent 5σ *g*-band limiting magnitude for different moon phases: New, Quarter, and Full Moon. The right-hand axis is the distance at which SSS17a would be detected given an apparent magnitude. The top axis is the search area that ASAS-SN can cover for a given exposure time per field using three of the five ASAS-SN sites and assuming fields are visible 5 h per night. If a candidate lies in the hatched region, ASAS-SN should not trigger based on SSS17a. The vertical cyan dashed line is the ASAS-SN exposure time in normal operations.

~ 160 Mpc. Of course, by the start of the next LVC run, the reference images will be deeper than shown in Fig. 7.

These restrictions mean we should only follow GW candidates with a distance $\leq 1.5 \times 10^{2.87 - 0.5 \log_{10}(\sqrt{A})}$ Mpc for a search region of $A \text{ deg}^2$. This limit is conservatively 50 per cent deeper than the one represented by the black line in Fig. 8, as SSS17a is only one example of a kilonova. With this new strategy, the majority of the events from LVC O3 would not have been triggered as they were too distant or their sky map areas were too large. Only three events, S190415z, S191213g, and S200213t, with minimum distances of 110, 136, and 134 Mpc, respectively, would have been observed by ASAS-SN under this strategy.

5 CONCLUSIONS

We described the ASAS-SN searches for EM counterparts of GW candidates detected by the Advanced LIGO/Virgo during the third science run (2019 April–2020 February). We observed a total of nine events, all with a >60 per cent probability of having at least one NS component. Unfortunately, like the rest of the community, ASAS-SN did not detect an optical counterpart. However, thanks to its large field of view and its five units located at four sites in both hemispheres, ASAS-SN covered an average of 50 per cent of the LVC search region in less than 24 h, starting a few minutes after the alert for some events. For seven events, ASAS-SN is the survey that covered the most area in 24 h with a g -band limiting magnitude of 18.5 mag. We were also able to trigger and observe the fields in the search region at a higher cadence, obtaining up to a dozen epochs within 24 h even for some of the larger search region. For LVC O4, we will only trigger on closer or well-localized sources: events where the distance D is smaller than $\sim 1.5 \times 10^{2.87-0.5 \log_{10}(\sqrt{A})}$ Mpc for a given search region spanning A deg 2 . With our new observational strategy, we will trigger on fewer objects but with a higher cadence and deeper observations.

With the additional Kagra detector and the LVC detector upgrades, the predicted rate of BNS merger detections will increase to 10_{-10}^{+52} yr $^{-1}$ from 1_{-1}^{+12} for O3 (Abbott et al. 2020) and the median search area will decrease to $33_{-5.3}^{+4.9}$ deg 2 (Abbott et al. 2020), roughly the same search area as for SSS17a. Even for an elongated shape, ASAS-SN should be able to map the full search region in only 2–5 pointings to a g -band depth of ~ 18.5 mag, taking only 5 min per field. With more epochs/exposure time, we will be able to reach a limiting magnitude of ~ 20.3 mag and detect candidates at distances up to ~ 160 Mpc assuming an SSS17a-like light curve. With LVK and our new observational strategy, ASAS-SN will play a key role in searching bright optical counterparts during the LVC O4 run and one of the few able to observe both hemispheres.

ACKNOWLEDGEMENTS

We thank the referee for the comments on the manuscript. Support for TdJ has been provided by NSF grants AST-1908952 and AST-1911074. BJS is supported by NSF grants AST-1907570, AST-1908952, AST-1920392, and AST-1911074. CSK and KZS are supported by NSF grants AST-1814440 and AST-1908570. Support for TW-SH was provided by NASA through the NASA Hubble Fellowship grant *HST-HF2-51458.001-A* awarded by the Space Telescope Science Institute, which is operated by the Association of Universities for Research in Astronomy, Inc., for NASA, under contract NAS5-265. JFB is supported by National Science Foundation grant no. PHY-2012955.

ASAS-SN is funded in part by the Gordon and Betty Moore Foundation through grants GBMF5490 and GBMF10501 to the Ohio State University, NSF grant AST-1908570, the Mt. Cuba Astronomical Foundation, the Center for Cosmology and AstroParticle Physics (CCAPP) at OSU, the Chinese Academy of Sciences South America Center for Astronomy (CAS-SACA), and the Villum Fonden (Denmark). Development of ASAS-SN has been supported by NSF grant AST-0908816, the Center for Cosmology and Astroparticle Physics, Ohio State University, the Mt. Cuba Astronomical Foundation, and by George Skestos. Some of the results in this paper have been derived using the HEALPY and HEALPIX packages.

This work is based on observations made by ASAS-SN. We wish to extend our special thanks to those of Hawaiian ancestry on whose sacred mountains of Maunakea and Haleakalā, we are privileged

to be guests. Without their generous hospitality, the observations presented herein would not have been possible.

Software used: ASTROPY (Astropy Collaboration et al. 2013), HEALPIX (Górski et al. 2005), HEALPY (Zonca et al. 2019), MATPLOTLIB (Hunter 2007), NUMPY (Harris et al. 2020), and SCIPY (Virtanen et al. 2020).

Facilities: Laser Interferometer Gravitational-Wave Observatory (USA), Virgo (Italy), Haleakala Observatories (USA), Cerro Tololo International Observatory (Chile), McDonald Observatory (USA), South African Astrophysical Observatory (South Africa).

DATA AVAILABILITY

All the BAYESTAR maps used in this work to produce the figures are public and available on the Gravitational-Wave Candidate Event Database (GraceDB) that is a service operated by the LIGO Scientific Collaboration (<https://gracedb.ligo.org/superevents/public/O3/>).

REFERENCES

Aartsen M. G. et al., 2017, *Astropart. Phys.*, 92, 30
 Aasi J. et al., 2015, *Classical Quantum Gravity*, 32, 115012
 Abbott B. P. et al., 2016, *Phys. Rev. Lett.*, 116, 061102
 Abbott B. P. et al., 2017a, *Phys. Rev. Lett.*, 119, 161101
 Abbott B. P. et al., 2017b, *Nature*, 551, 85
 Abbott B. P. et al., 2017c, *ApJ*, 848, L12
 Abbott B. P. et al., 2019, *Phys. Rev. X*, 9, 031040
 Abbott B. P. et al., 2020, *Living Rev. Relativ.*, 23, 3
 Abbott R. et al., 2021, *Phys. Rev. X*, 11, 021053
 Acernese F. et al., 2015, *Classical Quantum Gravity*, 32, 024001
 Ackley K. et al., 2019, *GCN Circ.*, 25654, 1
 Alard C., 2000, *A&AS*, 144, 363
 Alard C., Lupton R. H., 1998, *ApJ*, 503, 325
 Anand S. et al., 2019, *GCN Circ.*, 25706, 1
 Anand S. et al., 2020, *GCN Circ.*, 26767, 1
 Andreoni I. et al., 2017, *Publ. Astron. Soc. Aust.*, 34, e069
 Andreoni I. et al., 2019a, *GCN Circ.*, 26416, 1
 Andreoni I. et al., 2019b, *GCN Circ.*, 26424, 1
 Annala E., Gorda T., Kurkela A., Vuorinen A., 2018, *Phys. Rev. Lett.*, 120, 172703
 Antier S. et al., 2020, *MNRAS*, 497, 5518
 Arcavi I. et al., 2017, *Nature*, 551, 64
 Astropy Collaboration et al., 2013, *A&A*, 558, A33
 Bauswein A., Janka H. T., 2012, *Phys. Rev. Lett.*, 108, 011101
 Becerra R. L. et al., 2021, *MNRAS*, 507, 1401
 Bellm E. C. et al., 2019, *PASP*, 131, 018002
 Bertin E., Arnouts S., 1996, *A&AS*, 117, 393
 Brown T. M. et al., 2013, *PASP*, 125, 1031
 Buikema A. et al., 2020, *Phys. Rev. D*, 102, 062003
 Burbidge E. M., Burbidge G. R., Fowler W. A., Hoyle F., 1957, *Rev. Mod. Phys.*, 29, 547
 Cameron A. G. W., 1957, *PASP*, 69, 201
 Chambers K. C. et al., 2016, preprint ([arXiv:1612.05560](https://arxiv.org/abs/1612.05560))
 Chang S.-W. et al., 2021, *Publ. Astron. Soc. Aust.*, 38, e024
 Chornock R. et al., 2017, *ApJ*, 848, L19
 Connaughton V. et al., 2017, *GCN Circ.*, 21506, 1
 Coughlin M. W., 2020, *Nat. Astron.*, 4, 550
 Coughlin M. W. et al., 2020a, *MNRAS*, 492, 863
 Coughlin M. W. et al., 2020b, *MNRAS*, 497, 1181
 Coulter D. A. et al., 2017, *Science*, 358, 1556
 Covino S. et al., 2017, *Nat. Astron.*, 1, 791
 Cowperthwaite P. S. et al., 2017, *ApJ*, 848, L17
 Crisp H. et al., 2019, *GCN Circ.*, 25749, 1
 Díaz M. C. et al., 2017, *ApJ*, 848, L29
 Drout M. R. et al., 2017, *Science*, 358, 1570
 Ducoin J.-G. et al., 2019, *GCN Circ.*, 26558, 1

Dyer M. J., Dhillon V. S., Littlefair S., Steeghs D., Ulaczyk K., Chote P., Galloway D., Rol E., 2018, in Peck A. B., Seaman R. L., Benn C. R., eds, Proc. SPIE Vol. 10704, Observatory Operations: Strategies, Processes, and Systems VII. SPIE, Bellingham, p. 107040C

Ezquiaga J. M., Zumalacárregui M., 2017, *Phys. Rev. Lett.*, 119, 251304

Filippenko A. V., Li W. D., Treffers R. R., Modjaz M., 2001, in Paczynski B., Chen W.-P., Lemme C., eds, ASP Conf. Ser. Vol. 246, IAU Colloq. 183, Small Telescope Astronomy on Global Scales. Astron. Soc. Pac., San Francisco, p. 121

Flaugher B. et al., 2015, *AJ*, 150, 150

Goldstein A. et al., 2017, *ApJ*, 848, L14

Gompertz B. P. et al., 2020, *MNRAS*, 497, 726

Górski K. M., Hivon E., Banday A. J., Wandelt B. D., Hansen F. K., Reinecke M., Bartelmann M., 2005, *ApJ*, 622, 759

Graham M. J. et al., 2020, *Phys. Rev. Lett.*, 124, 251102

Harris C. R. et al., 2020, *Nature*, 585, 357

Hunter J. D., 2007, *Comput. Sci. Eng.*, 9, 90

Kasen D., Metzger B., Barnes J., Quataert E., Ramirez-Ruiz E., 2017, *Nature*, 551, 80

Kasliwal M. M. et al., 2020a, *ApJ*, 905, 145

Kasliwal M. M. et al., 2020b, GCN Circ., 27051, 1

Kawabata M., 2020, Transient Name Server Classification Report, 2020-499, 1

Kilpatrick C. D. et al., 2017, *Science*, 358, 1583

Kochanek C. S. et al., 2017, *PASP*, 129, 104502

Levan A. J., Jonker P. G., 2020, *Nat. Rev. Phys.*, 2, 455

Li L.-X., Paczyński B., 1998, *ApJ*, 507, L59

LIGO Scientific Collaboration, Virgo Collaboration, 2019a, GCN Circ., 24168, 1

LIGO Scientific Collaboration, Virgo Collaboration, 2019b, GCN Circ., 24237, 1

LIGO Scientific Collaboration, Virgo Collaboration, 2019c, GCN Circ., 25606, 1

LIGO Scientific Collaboration, Virgo Collaboration, 2019d, GCN Circ., 25695, 1

LIGO Scientific Collaboration, Virgo Collaboration, 2019e, GCN Circ., 25814, 1

LIGO Scientific Collaboration, Virgo Collaboration, 2019f, GCN Circ., 26350, 1

LIGO Scientific Collaboration, Virgo Collaboration, 2019g, GCN Circ., 26402, 1

LIGO Scientific Collaboration, Virgo Collaboration, 2020a, GCN Circ., 26759, 1

LIGO Scientific Collaboration, Virgo Collaboration, 2020b, GCN Circ., 27042, 1

Lipunov V. M. et al., 2017, *ApJ*, 850, L1

Lundquist M. J. et al., 2019, *ApJ*, 881, L26

McBrien O. et al., 2019, GCN Circ., 24197, 1

McCullly C. et al., 2017, *ApJ*, 848, L32

Margalit B., Metzger B. D., 2017, *ApJ*, 850, L19

Metzger B. D., 2019, *Living Rev. Relativ.*, 23, 1

Metzger B. D. et al., 2010, *MNRAS*, 406, 2650

Moesta P., Alic D., Rezzolla L., Zanotti O., Palenzuela C., 2012, *ApJ*, 749, L32

Nicholl M. et al., 2017, *ApJ*, 848, L18

Palenzuela C., Lehner L., Yoshida S., 2010, *Phys. Rev. D*, 81, 084007

Paterson K. et al., 2021, *ApJ*, 912, 128

Petrov P. et al., 2021, preprint ([arXiv:2108.07277](https://arxiv.org/abs/2108.07277))

Pian E. et al., 2017, *Nature*, 551, 67

Piro A. L., Kollmeier J. A., 2018, *ApJ*, 855, 103

Rubin D., Szapudi I., Shappee B. J., Anand G. S., 2020, *ApJ*, 890, L6

Sakstein J., Jain B., 2017, *Phys. Rev. Lett.*, 119, 251303

Schlafly E. F., Finkbeiner D. P., 2011, *ApJ*, 737, 103

Schutz B. F., 1986, *Nature*, 323, 310

Shappee B. J. et al., 2014, *ApJ*, 788, 48

Shappee B. J. et al., 2017, *Science*, 358, 1574

Shappee B. J. et al., 2019a, GCN Circ., 24309, 1

Shappee B. J. et al., 2019b, GCN Circ., 24313, 1

Shappee B. J. et al., 2019c, GCN Circ., 24323, 1

Singer L. P., Price L. R., 2016, *Phys. Rev. D*, 93, 024013

Smartt S. J. et al., 2017, *Nature*, 551, 75

Smith K. W. et al., 2019, GCN Circ., 24210, 1

Soares-Santos M. et al., 2017, *ApJ*, 848, L16

Steeghs D. et al., 2019a, GCN Circ., 24224, 1

Steeghs D. et al., 2019b, GCN Circ., 24291, 1

Stein R. et al., 2019, GCN Circ., 25656, 1

Tony J. L. et al., 2018, *PASP*, 130, 064505

Troja E. et al., 2017, *Nature*, 551, 71

Turpin D. et al., 2019, GCN Circ., 25847, 1

Utsumi Y. et al., 2017, *PASJ*, 69, 101

Valenti S. et al., 2017, *ApJ*, 848, L24

Villar V. A. et al., 2017, *ApJ*, 851, L21

Virtanen P. et al., 2020, *Nat. Methods*, 17, 261

White D. J., Daw E. J., Dhillon V. S., 2011, *Classical Quantum Gravity*, 28, 085016

Zonca A., Singer L., Lenz D., Reinecke M., Rosset C., Hivon E., Gorski K., 2019, *J. Open Source Softw.*, 4, 1298

APPENDIX A:

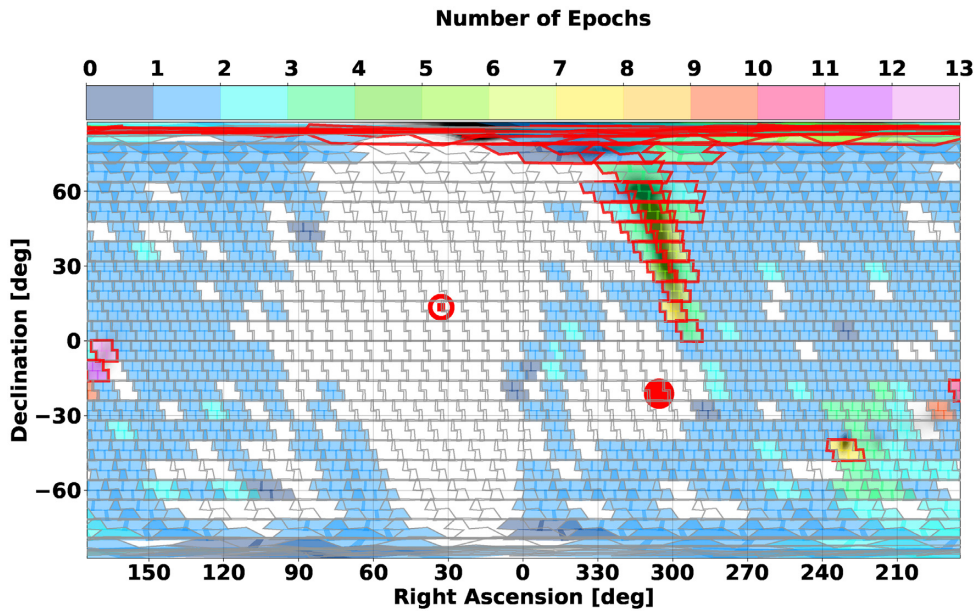


Figure A1. Same as Fig. 4, except for LVC event S190426c.

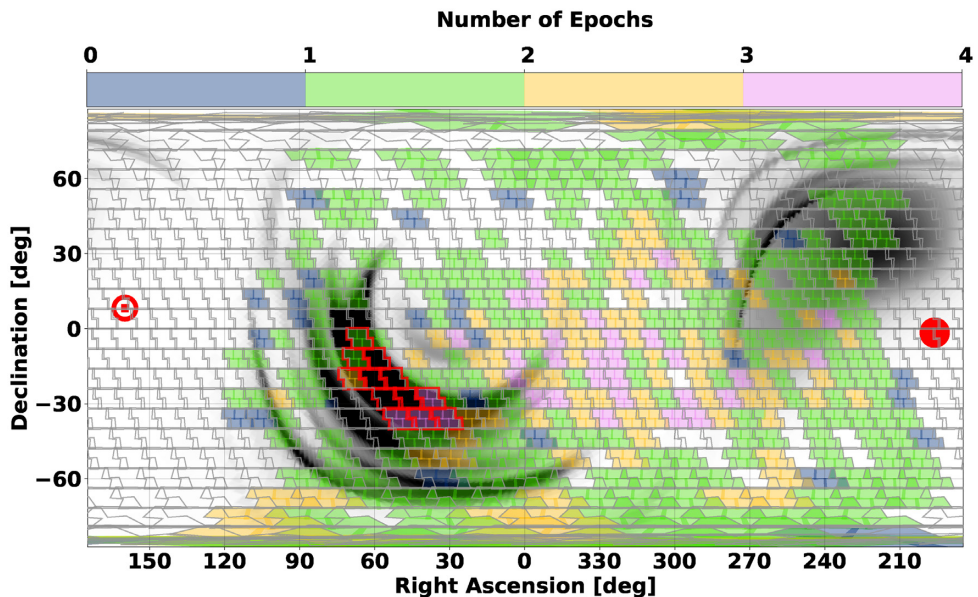


Figure A2. Same as Fig. 4, except for LVC event S190901ap.

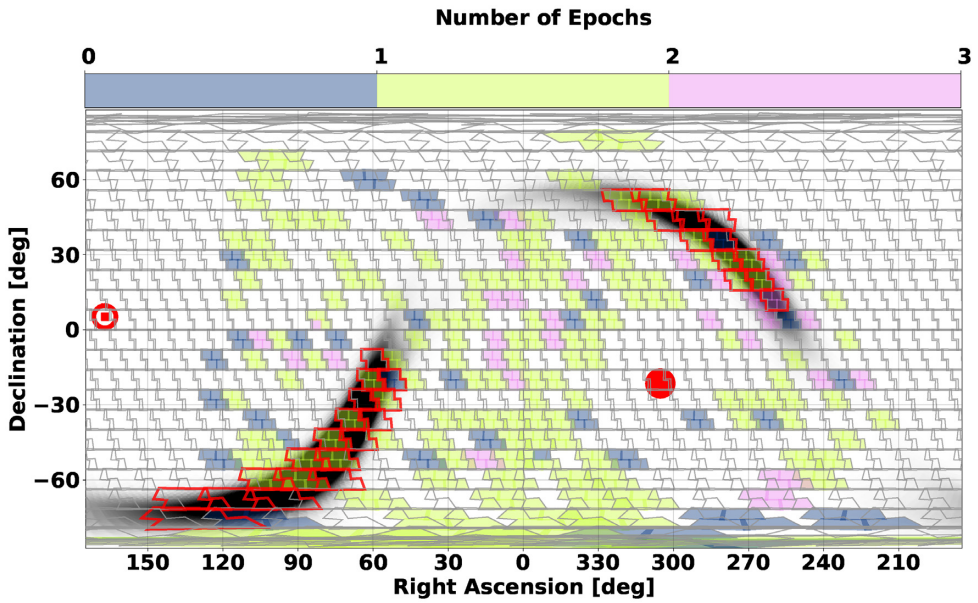


Figure A3. Same as Fig. 4, except for LVC event S190910d.

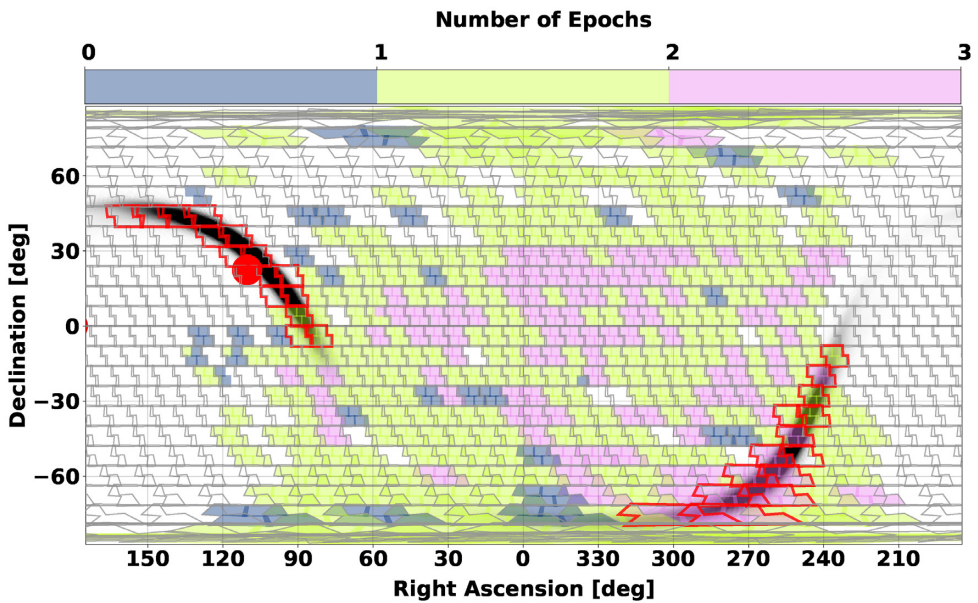


Figure A4. Same as Fig. 4, except for LVC event S190923y.

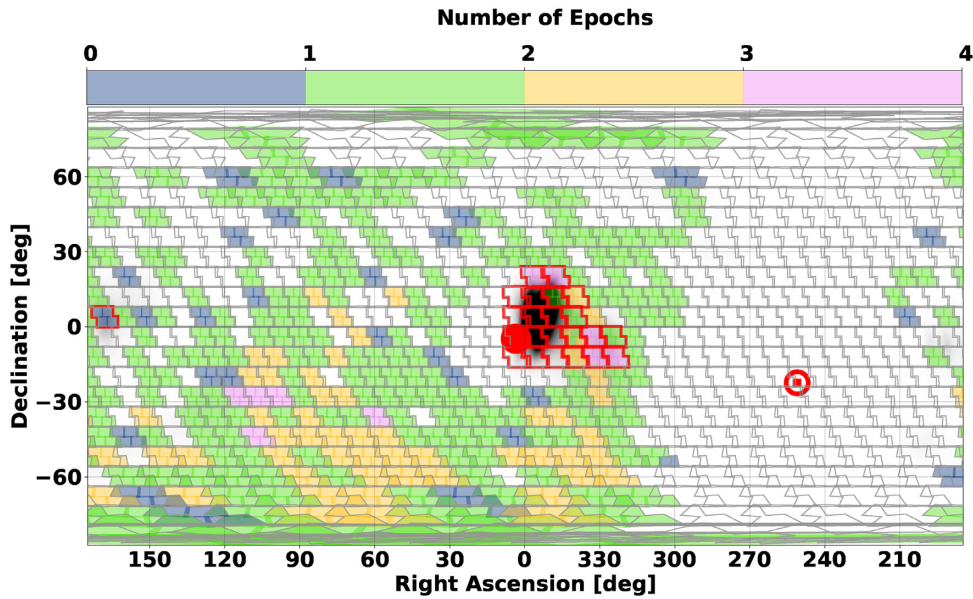


Figure A5. Same as Fig. 4, except for LVC event S191205ah.

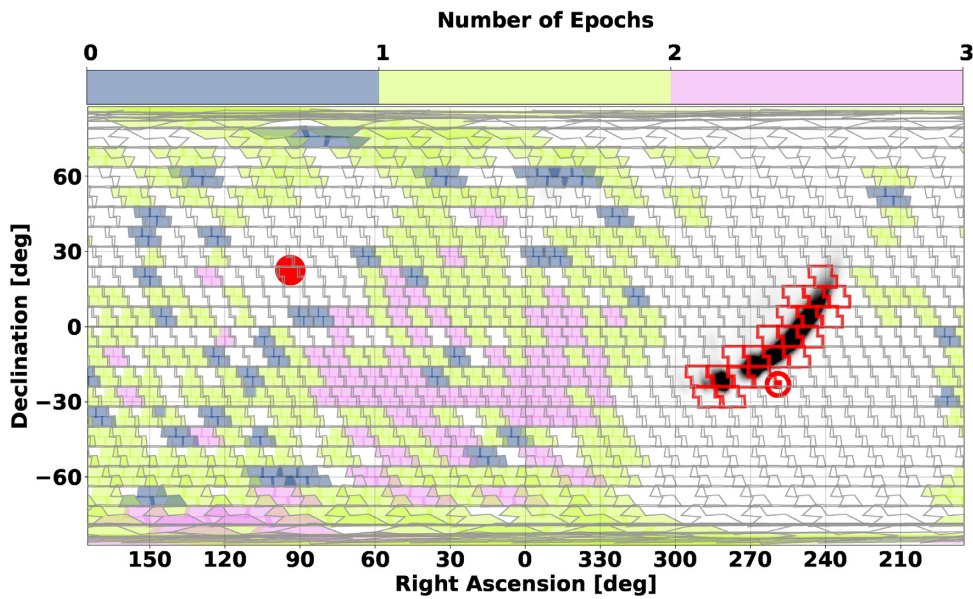


Figure A6. Same as Fig. 4, except for LVC event S191213g. This candidate was not observable due to our Sun and our hour angle limits.

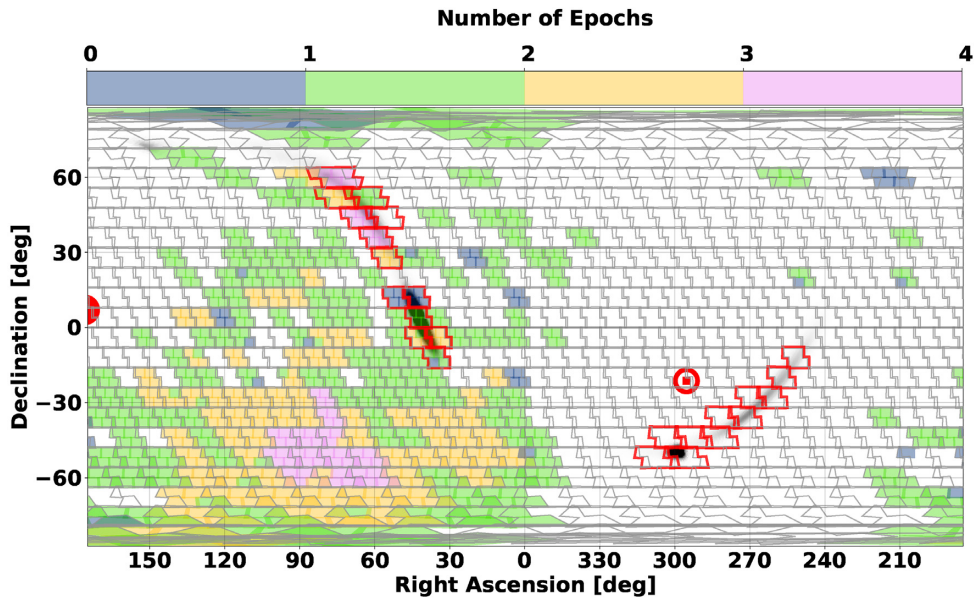


Figure A7. Same as Fig. 4, except for LVC event S200115j.

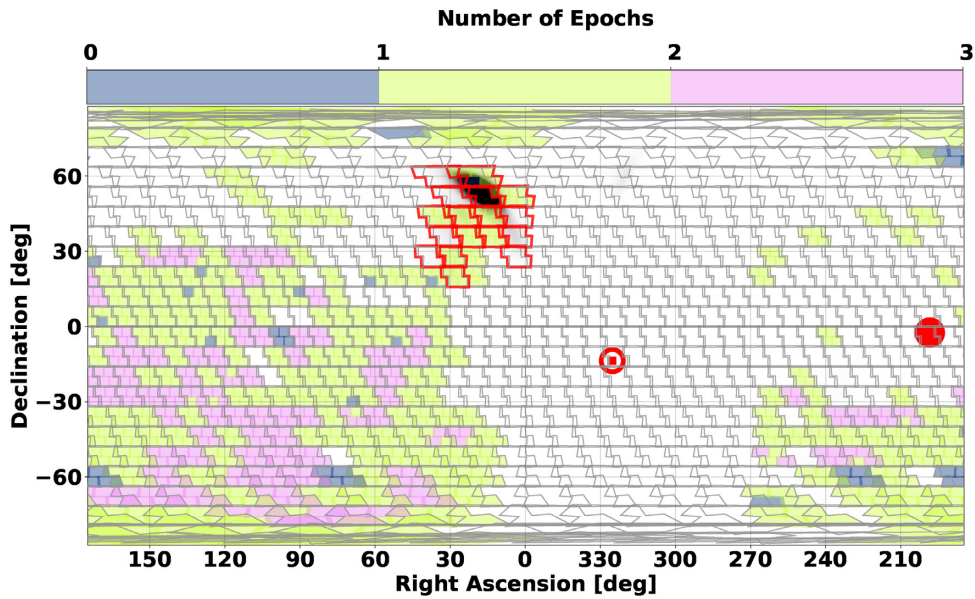


Figure A8. Same as Fig. 4, except for LVC event S200213t.

This paper has been typeset from a $\text{\TeX}/\text{\LaTeX}$ file prepared by the author.